


Topological phases induced by the Aubry-André-Harper potential in the longer-range Kitaev superconducting chain

Chunhui Zhang , Li Sheng,^{*} and Dingyu Xing

Department of Physics, National Laboratory of Solid State Microstructures, Collaborative Innovation Center of Advanced Microstructures, Nanjing University, Nanjing 210093, China

 (Received 17 April 2022; revised 8 July 2022; accepted 31 August 2022; published 13 September 2022)

We investigate the one-dimensional longer-range Kitaev chain with an on-site complex Aubry-André-Harper (AAH) potential. For the incommensurate (commensurate) case, by calculating the real-space (Bloch) winding number and energy spectrum we discover the AAH potential-induced phases and present the related phase diagrams. We also find that the imaginary phase shift in AAH potentials can suppress these topological phases for both cases. For the incommensurate case, the inverse participate ratios of the eigenstates with the smallest $|E|$ s indicate the existence of the incommensurate AAH potential-induced phases, and the result of the mean inverse participate ratio shows that these incommensurate AAH potential-induced phases are not always strongly localized.

DOI: [10.1103/PhysRevB.106.094203](https://doi.org/10.1103/PhysRevB.106.094203)

I. INTRODUCTION

Recently, Majorana zero modes [1] have received much interest due to their non-Abelian statistics [2,3] and the potential of topological quantum computation [4]. Among the proposals for realizing the Majorana zero modes, the one-dimensional topological superconductor (1D TSC) has been intensively studied in the past few years [5–11]. The first model describing the 1D TSC is Kitaev's 1D spinless p -wave superconductor [5]. Under the open boundary conditions (OBCs), this model is topologically nontrivial, and the Majorana zero modes can exist at each end of the chain.

In Kitaev's pioneering work, only the nearest hopping and pairing terms are included in the model. However, recent studies have pointed out that taking the longer-range hopping and pairing term is reasonable due to the finite range of hybridization of the electron wave function and Cooper pairing [12,13]. It has also been found that the 1D spinless TSC with the next-nearest hopping and pairing term can be connected with the transverse field Ising model with three spin interactions and enables us to investigate both the local and nonlocal qubits [12,14,15]. Besides, several studies have shown that the topological states with longer-range hopping and pairing terms and random disorders can have higher topological invariant and have richer phase diagrams [12–14,16,17].

In the community of the TSC, the interplay of the disorder and topology in a 1D Kitaev chain with periodic and quasiperiodic potential is also an important topic because it is related to the robustness of Majorana zero modes against disorders [18,19], which is critical to the error-free topological quantum computation. And many works about the 1D Kitaev chain with quasiperiodic potentials devote to the transition

from the topological to the topologically trivial phase [20–24], quench dynamics [25,26], and quantum criticality [27].

Up to now, we focus on the Hermitian case and recent studies have found that the non-Hermitian Hamiltonian can be employed to describe many physical systems [28–42] and has many novel properties, such as the exceptional point [39,42–47], the revised bulk-boundary correspondence [48–53], and the non-Hermitian skin effect [48,49,54–58]. Based on these motivations, growing efforts have been paid to investigate the interplay between the non-Hermiticity and Anderson localization in quasiperiodic systems [59–73].

As far as we know, on the one hand, most present works about the 1D TSC with (quasi)periodic potentials only care about the nearest hopping and pairing terms. And they usually focus on the transitions from the TSC phase to Anderson localized phases induced by the quasiperiodic potential; On the other hand, random disorders can introduce topological phases in the topological states with the nearest hopping and pairing terms [12–14,17]. Besides, both random disorders and the quasiperiodic potential can introduce inhomogeneity and cause Anderson localization [74,75]. However, the study about the interplay between the quasiperiodic potential and the longer-range Kitaev chain is still lacking, and the quasiperiodic potential-induced topological phases in superconductors are also uncovered, which motivates us to investigate whether the quasiperiodic potential can induce topological phases in the 1D TSC with the longer-range term, such as random disorders. If so, what is the difference between the topological phases induced by quasiperiodic potentials and ones induced by random disorders?

In this paper, we consider the longer-range Kitaev SC chain with a complex Aubry-André-Harper (AAH) potential introduced by the imaginary phase shift. For both incommensurate and commensurate cases, we reveal the topological phases induced by the complex AAH potential. We find that the AAH potential-induced topological phases do not always require

^{*}shengli@nju.edu.cn

obvious Anderson localization, which is different from the topological Anderson phase induced by the random disorders in previous works [76–79]. We also find that the imaginary phase shift can suppress the AAH potential-induced topological phases.

This paper is organized as follows: In Sec. II, we review the topological phase diagrams of the longer-range Kitaev SC chain and discuss the symmetry and topological classes of the model with the complex AAH potential. In Sec. III, after introducing the corresponding real-space winding number, we present the numerical results about the incommensurate AAH potential-induced topological phase in Sec. III A, which includes the real-space winding number, the spectrum of energy modulus $|E|$, and the density distribution of eigenstates with the four smallest energy modulus $|E|$. To support the existence of incommensurate AAH potential-induced topological phase, we also show results of the participation ratio (MIPR) and the related mean inverse participation ratio (IPR) in Sec. III B. The commensurate AAH potential-induced topological phase is also displayed and discussed in Sec. IV. Finally, we perform a summary in Sec. V.

II. MODEL

Let us begin with the following Hermitian longer-range Kitaev chain model [12–14],

$$H_0 = -2\mu \sum_{n=1}^L c_n^\dagger c_n - \Delta_1 \sum_{n=1}^{L-1} (c_n^\dagger c_{n+1} - c_n c_{n+1} + \text{H.c.}) - \Delta_2 \sum_{n=1}^{L-1} (c_n^\dagger c_{n+2} - c_n c_{n+2} + \text{H.c.}), \quad (1)$$

where c_n is the annihilation operator of the spinless fermion at the n th site. The strength of the real chemical potential is 2μ . The Δ_1 (Δ_2) corresponds to the strength of the nearest- (next-nearest-) equal hopping and SC pairing.

Before introducing the non-Hermitian term, let us discuss the topological phase diagram of the model given by Eq. (1). To this end, we perform the Fourier transformation to obtain the following Hamiltonian in momentum space:

$$H_0(k) = \frac{1}{2} \sum_{k \in \text{BZ}} \psi_k^\dagger \tilde{H}_0(k) \psi_k, \quad (2)$$

with the Nambu basis $\psi_k = (c_k, c_{-k}^\dagger)^T$ and the single-particle Hamiltonian,

$$\tilde{H}_0(k) = -g_z(k)\tau_z + g_y(k)\tau_y, \quad (3)$$

where τ_y and τ_z are Pauli matrices acting on the Nambu space, $g_z(k) = \mu + \Delta_1 \cos k + \Delta_2 \cos 2k$ and $g_y(k) = \Delta_1 \sin k + \Delta_2 \sin 2k$. Next, we introduce the following transformation:

$$U = \frac{1}{\sqrt{2}} \begin{pmatrix} 1 & 1 \\ i & -i \end{pmatrix}. \quad (4)$$

Then, we have the following off-diagonal matrix:

$$U \tilde{H}_0(k) U^\dagger = i \begin{pmatrix} 0 & -g_z(k) + ig_y(k) \\ g_z(k) + ig_y(k) & 0 \end{pmatrix}, \quad (5)$$

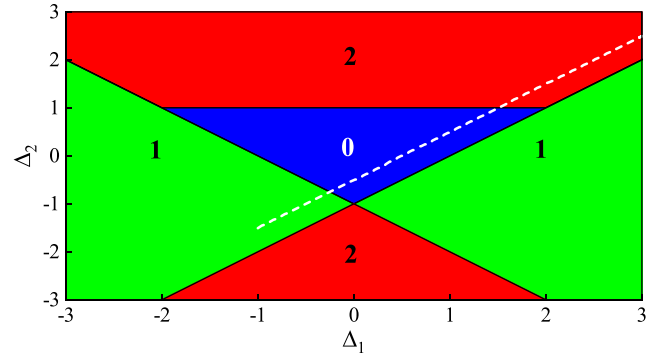


FIG. 1. Phase diagram of the system in the $V = 0$ case. The numbers in the figure denote the winding number from Eq. (6). Here we set $\mu = 1.0$. The white dashed line is $\Delta_2 = \Delta_1 - 0.5$ with $\Delta_1 \in [-1, 3]$.

and the winding number is given by

$$\begin{aligned} \nu &= \frac{1}{2\pi i} \int_{-\pi}^{\pi} dk \partial_k [g_z(k) + ig_y(k)] \\ &= \frac{1}{2\pi i} \int_{-\pi}^{\pi} dk \partial_k [\ln(\mu + \Delta_1 e^{ik} + \Delta_2 e^{2ik})]. \end{aligned} \quad (6)$$

We find that $\nu = 1$ for $(\Delta_2 - \Delta_1 + \mu)(\Delta_2 + \Delta_1 + \mu) < 0$; $\nu = 2$ for $(\Delta_2 - \Delta_1 + \mu)(\Delta_2 + \Delta_1 + \mu) > 0$, $(\mu - \Delta_2)(\Delta_2 \pm \Delta_1 + \mu) < 0$, and $\nu = 0$ for another case (see Appendix A). In the following part, we set $\mu = 1.0$ as the energy unit. The corresponding phase diagram is presented in Fig. 1, which is the same as the one of the longer-range SSH chain [16,17].

Then, we consider the following complex AAH potential:

$$H_1 = -V \sum_n^L \cos(2\pi\alpha n - i\beta) c_n^\dagger c_n, \quad (7)$$

where V is the strength of the potential, $1/\alpha$ gives the period of the AAH potential, and $-i\beta$ is an imaginary shift in the potential. Under the Nambu basis,

$$\psi = (c_1, c_2, \dots, c_{N-1}, c_N, c_1^\dagger, c_2^\dagger, \dots, c_{N-1}^\dagger, c_N^\dagger)^T, \quad (8)$$

$H = H_0 + H_1$ can be written as $H = \psi^\dagger \tilde{H} \psi / 2$. We can check that single-particle Hamiltonian \tilde{H} possesses the following symmetry:

$$C \tilde{H}^T C^{-1} = -\tilde{H}, \quad S \tilde{H} S^{-1} = -\tilde{H}, \quad (9)$$

with particle-hole symmetry (PHS) operator $C = \mathbb{1}_N \otimes \tau_x$ and sublattice symmetry (SLS) $S = \mathbb{1}_N \otimes \tau_x$. So this model belongs to class D and the SLS commutes with the PHS [80].

III. INCOMMENSURATE CASES

Let us begin with the commensurate case. Here $\alpha = (\sqrt{5} - 1)/2$ is the golden ratio number, and the model is quasiperiodic. Since this model has the non-Hermitian SLS $S \tilde{H} S^{-1} = -\tilde{H}$, we can adopt the following real-space winding number method [81–83] to investigate the topological transition,

$$\nu = \frac{1}{4L'} \text{Tr}'(SQ[Q, X]) + \text{H.c.}, \quad (10)$$

where X is the coordinate operator X . The Q matrix can be given by

$$Q = \sum_n (|\psi_{R,n}\rangle\langle\psi_{L,n}| - |\psi'_{R,n}\rangle\langle\psi'_{L,n}|). \quad (11)$$

Here n is the band index and $|\psi_{R,n}\rangle$ and $|\psi_{L,n}\rangle$ are the right and left eigenvectors satisfying

$$\tilde{H}|\psi_{R,n}\rangle = E_n|\psi_{R,n}\rangle, \quad \tilde{H}^\dagger|\psi_{L,n}\rangle = E_n^*|\psi_{L,n}\rangle. \quad (12)$$

And $|\psi_{R,n}\rangle$ and $|\psi'_{R,n}\rangle$ are SLS partners: When a right eigenvector $|\psi_{R,n}\rangle$ satisfies $\tilde{H}|\psi_{R,n}\rangle = E_n|\psi_{R,n}\rangle$, we can also find a right eigenvector $|\psi'_{R,n}\rangle = S|\psi_{R,n}\rangle$ satisfying $\tilde{H}|\psi'_{R,n}\rangle = -E_n|\psi'_{R,n}\rangle$. (This is also valid for left eigenvectors.) The chain length L includes the two boundary intervals $1 \leq x \leq l$ and $L-l+1 \leq x \leq L$ and the middle interval with length $L' = L - 2l$. For the $L \rightarrow \infty$ limit $\nu \rightarrow 1$ when a system is topological and 0 for the trivial phase. And Tr' stands for the sum over the middle interval and the Nambu index.

A. Incommensurate AAH potential-induced topological phase

Let us begin with $\beta = 0$, i.e., Hermitian cases. Here we consider the $\Delta_2 = \Delta_1 - 0.5$ with $\Delta_1 \in [-1, 3]$ (the white dashed lines in Fig. 1) and set the chemical potential $\mu = 1.0$. The real-space winding number as a function of V and Δ_1 are shown in Fig. 2(a). We find that there are two types of the topological transition involving the AAH potential-induced topological phases: (a) The topological transition from the normal superconductor (NSC) to the AAH potential-induced TSC including $\nu = 0 \rightarrow 1$ and $\nu = 0 \rightarrow 1 \rightarrow 2$. (b) The topological transition from TSC to AAH potential-induced TSC including $\nu = 2 \rightarrow 1$.

In Figs. 2(b1) and 2(b2), we show the real-space winding number ν and spectra under the open boundary conditions as functions of the incommensurate AAH potential strength V with $\Delta_1 = 1.4$, $\Delta_2 = 0.9$, and $\beta = 0$. We first focus on Fig. 2(b1). As the potential strength V increases, the AAH potential-induced topological phases can be identified when $1.4 \leq V \leq 3.4$. In this topological region, $\nu = 1$ for $V \approx 1.4$ and $V \approx 3.4$; the $\nu = 2$ plateau exists when $1.8 \leq V \leq 3$; The topological transition $\nu = 1 \rightarrow 2$ ($\nu = 2 \rightarrow 1$) happens when $1.4 < V < 1.8$ ($3 < V \leq 3.4$). The spectra under the OBCs in Fig. 2(b2) also show the existence of the incommensurate AAH potential induce topological phases: The region where the Majorana zero modes occur matches well with the topological region $1.4 \leq V \leq 3.4$ in Fig. 2(b1). Thus, both results indicate that the AAH potential can drive the longer-range Kitaev chain (with $\Delta_1 = 1.4$, $\Delta_2 = 0.9$, and $\beta = 0$) from the NSC phase to the TSC phase when $1.4 \leq V \leq 3.4$.

After discussing the Hermitian limit, we take the imaginary phase shift $i\beta$ into account, which introduces the non-Hermiticity in the model. In Figs. 2(c1) and 2(c2), we show the phase diagram about V and Δ_1 . (Here, we take $\Delta_1 = 1.4$, $\Delta_2 = 0.9$, and $\beta = 0.4$.) Comparing with the results in Figs. 2(b1) and 2(b2), it is found that the topological phase with $2.2 < V \leq 3.4$ is suppressed whereas the topological region with $1.4 \leq V \leq 2.2$ is almost unchanged when $\beta = 0.4$. The phase diagram about varying β and V in Fig. 2(d) is also shown in Fig. 2(d). As the β increases, we find that the AAH potential-induced topological phase with larger AAH

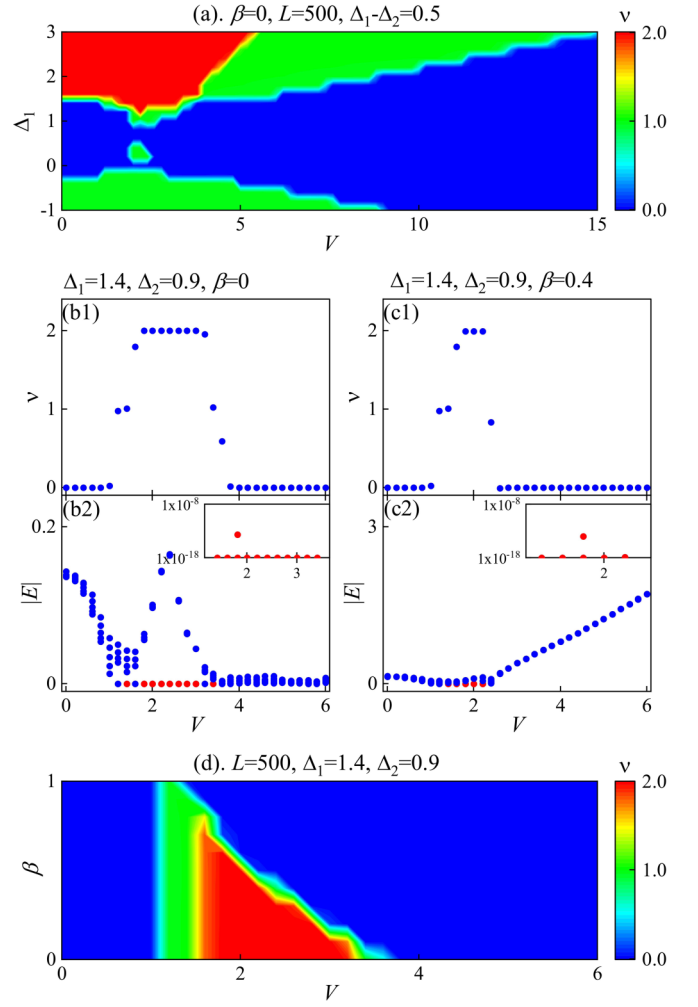


FIG. 2. (a) The real-space winding number ν as a function of the AAH potential strength V and Δ_1 ($\Delta_2 = \Delta_1 - 0.5$). (b1)–(c1) The real-space winding number ν as a function of the AAH potential strength V . (b2)–(c2) Spectra of the energy levels with the ten smallest $|E|$ s under OBCs as functions of the AAH potential strength V . Red points are zero modes. The inset figure shows the enlarged topological region. (The eigenmodes with $|E| > 10^{-8}$ are not shown.) (d) The real-space winding number ν as a function of the AAH potential strength V and β . Other parameters are lattice strength $L = 500$, the length of the boundary interval $l = 100$, and $\alpha = [\sqrt{5} - 1]/2$.

potential strength V is easier to be suppressed than the one with the smaller potential strength V . And the phase boundaries in the $\nu = 0 \rightarrow 1$ and $\nu = 1 \rightarrow 2$ transitions are almost the same for varying β until the corresponding AAH potential-induced TSC phases are removed. Apart from the NSC \rightarrow AAH potential-induced TSC transition, similar suppression effects of β in an example of the TSC \rightarrow AAH potential-induced TSC transition are shown in Appendix. B.

At the end of this subsection, we discuss the density distribution of the following normalized eigenstate:

$$|\psi_m\rangle = \sum_{n=1}^L (u_{m,n}c_{m,n} + v_{m,n}c_{m,n}^\dagger)|0\rangle, \quad (13)$$

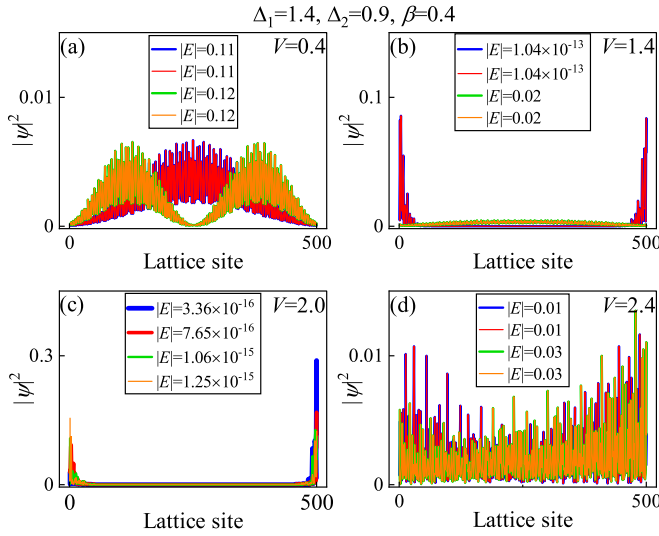


FIG. 3. Density distributions of the eigenstates with the four smallest $|E|$ s. The parameters are $\Delta_1 = 1.4$, $\Delta_2 = 0.9$, $\beta = 0.4$, and $V = 0.4, 1.4, 2.0, 2.4$ in (a)–(d), correspondingly. Other parameters are $\mu = 1.0$ and lattice strength $L = 500$.

where m is the band index and n denotes the n th site. Then, the corresponding density distribution at the n th site is

$$|\psi_{m,n}|^2 = |u_{m,n}|^2 + |v_{m,n}|^2. \quad (14)$$

Since $\nu_{\max} = 2$, the system has four zero-edge modes at most. So we consider the four eigenstates with the four smallest $|E|$ s. When the system is topological, the corresponding edge modes occur. In Fig. 3, we take $(\Delta_1, \Delta_2, \beta) = (1.4, 0.9, 0.4)$ and $V = 0.4, 1.4, 2.0, 2.4$ cases as examples and display the density distribution of these eigenstates. When $V = 0.4$, the system is topologically trivial and has no zero-edge modes; then, the system has two zero modes for $V = 1.4$ and four zero-edge modes for the $V = 2.0$ case, which indicates that the system is in $\nu = 1$ and $\nu = 2$ topological phases, correspondingly. Finally, the system has no zero-edge modes and is in a trivial phase when $V = 2.4$. These results are also consistent with the ones shown in Figs. 2(c1) and 2(c2).

B. Localization properties

In this section, we discuss the localization properties of this model. To this end, we calculate the IPR and MIPR which have been adopted to investigate localization properties of the standard 1D p -wave Kitaev SC chain with Hermitian [20,23,24] and non-Hermitian quasiperiodic potential [63,70–73]. For the m th right eigenstate $|\psi\rangle_{m,R} = \sum_j (u_j c_j + v_j c_j^\dagger)|0\rangle_R$, the corresponding IPR I_m is

$$I_m = \frac{\sum_{n=1}^L (|u_{m,n}|^4 + |v_{m,n}|^4)}{[\sum_{n=1}^L (|u_{m,n}|^2 + |v_{m,n}|^2)]^2}, \quad (15)$$

where n is the site index. It is known that the $I_m \rightarrow 1$ when the eigenstate is extended and $I_m \rightarrow 1/(2L)$ when the eigenstate is localized. Then, we can also define the MIPR $\bar{I} = (\sum_{m=1}^{2L} I_m)/(2L)$. Still, for the extended system $\bar{I} \rightarrow 1/(2L)$, whereas $\bar{I} \rightarrow 1$ for the localized system.

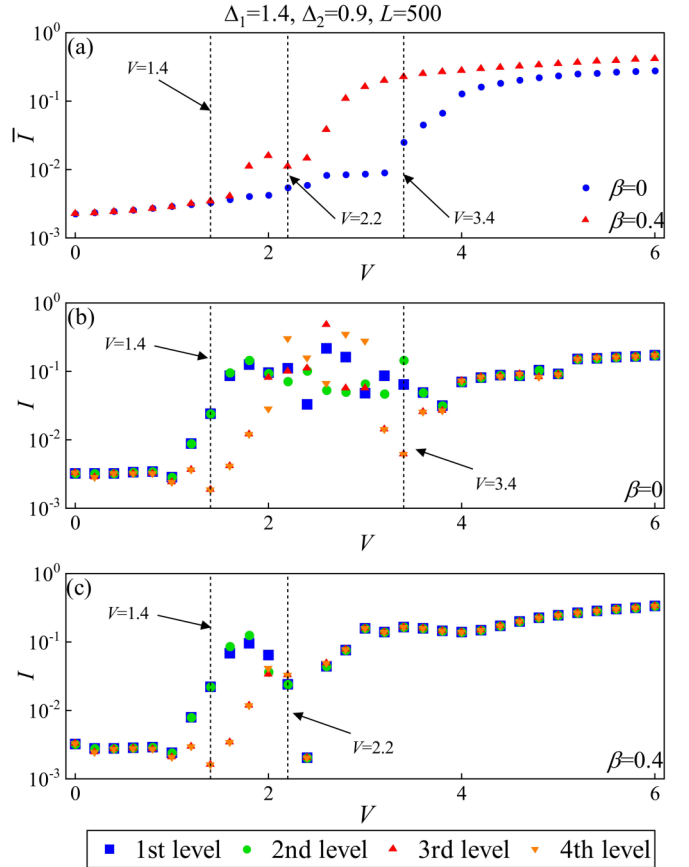


FIG. 4. (a): MIPRs under OBC with varying quasiperiodic potential strength V and $\beta = 0, 0.4$. (b) and (c): IPRs of the energy bands with the four smallest $|E|$ s and OBCs as functions of varying quasiperiodic potential strength V . Here $\beta = 0$ in (b) and 0.4 in (c). The black dashed lines in (a)–(c) denote the phase boundaries given by the real-space winding number. Other parameters are $\Delta_1 = 1.4$, $\Delta_2 = 0.9$, $\mu = 1.0$, and $L = 500$.

In Fig. 4(a), we show the MIPR \bar{I} of our model with $(\Delta_1, \Delta_2) = (1.4, 0.9)$ and $\beta = 0, 0.4$ as functions of V under OBC. For $\beta = 0$ cases, we find that $\bar{I} < 10^{-2}$ when $0 \leq V \leq 3.2$, which means that the Hermitian AAH potential-induced topological phase with $1.4 \leq V \leq 3.2$ is *not* strongly Anderson localized (note that $L = 500$ so \bar{I} is of the order 10^{-3} for extended states). Then, $\bar{I} > 10^{-2}$ and continues to increase when $V > 3.2$, which indicates that the system becomes a localized phase and only the $V \approx 3.4$ Hermitian AAH potential-induced topological phase is a localized phase.

As for the $\beta = 0.4$ case, its $\bar{I} > 10^{-2}$ when $V \geq 1.8$, which indicates that the system with $\beta = 0.4$ is easier to be localized, and the non-Hermitian AAH potential-induced topological phase with $\beta = 0.4$ tends to be more localized than the Hermitian case with $\beta = 0$ when $1.8 \leq V \leq 2.2$. The IPRs of eigenstates with the four smallest $|E|$ s are also shown in Figs. 4(b) and 4(c). Still, we consider the *four* smallest $|E|$ s since the maximum of $\nu = 2$. When $1.4 \leq V \leq 3.4$ from Fig. 4(b), we find that the first and second eigenstates' IPRs are relatively large ($I > 10^{-2}$), whereas the third and fourth eigenstates' IPRs $I \sim 10^{-3} \rightarrow 10^{-1} \rightarrow 10^{-3}$ in the topological region. Since the system is not strongly

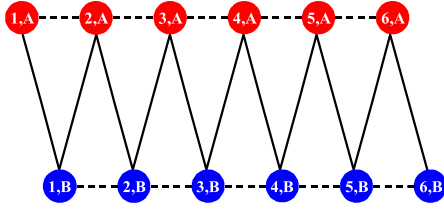


FIG. 5. Schematic of the longer-range Kitaev chain with $\alpha = 1/2$ AAH potentials given by Eq. (16). For the n th lattice in $H = H_0 + H_1$, this lattice belongs to the sublattice $A(B)$ when m is odd (even), which is marked by a filled red (blue) circle. The solid (dashed) lines represent the nearest (next-nearest) hopping and superconducting pairing term.

Anderson localized, the increase in these IPRs indicates that these eigenstates are edge states, and the AAH induced $\nu = 1$ and 2 topological phases exist in this case. Similar results can be found in Fig. 4(c) when $1.4 \leq V \leq 2.2$ and $\beta = 0.4$.

IV. COMMENSURATE CASE

When α is rational, the AAH potential is commensurate, and the Anderson localization transition will not occur in the system. Here, we discuss $\alpha = 1/2$ case. In this case, Eq. (1) can be rewritten as

$$\begin{aligned}
 H = & V \cosh \beta \sum_n (c_{n,A}^\dagger c_{n,A} - c_{n,B}^\dagger c_{n,B}) \\
 & - \Delta_1 \sum_n (c_{n,A}^\dagger c_{n,B} + c_{n,B}^\dagger c_{n+1,A} - c_{n,A} c_{n,B} \\
 & - c_{n,B} c_{n+1,A} + \text{H.c.}) \\
 & - \Delta_2 \sum_{n,\sigma=A,B} (c_{n,\sigma}^\dagger c_{n+1,\sigma} - c_{n,\sigma} c_{n+1,\sigma} + \text{H.c.}) \\
 & - 2\mu \sum_{n,\sigma=A,B} c_{n,\sigma}^\dagger c_{n,\sigma}, \quad (16)
 \end{aligned}$$

where $\sigma = A(B)$ is the sublattice index corresponding to the odd (even) lattice of the original longer-range Kitaev chain with the AAH potential. The corresponding illustration of Eq. (16) is shown in Fig. 5. To characterize the topological properties of this model, we have to calculate the topological invariants. Due to the periodic nature of $\alpha = 1/2$ AAH potential, the winding number can be obtained in the momentum space. With the Nambu basis,

$$\Psi = (c_{k,A}, c_{k,B}, c_{-k,A}^\dagger, c_{-k,B}^\dagger)^T. \quad (17)$$

The Hamiltonian is $H(k) = \frac{1}{2} \sum_{k \in \text{BZ}} \Psi_k^\dagger \tilde{H}(k) \Psi_k$ where

$$H(k) = \begin{pmatrix} -M_-(k) & -z(k) & q(k) & -w(k) \\ -z^*(k) & -M_+(k) & w^*(k) & q(k) \\ q^*(k) & w(k) & M_-(k) & z(k) \\ -w^*(k) & q^*(k) & z^*(k) & M_+(k) \end{pmatrix}, \quad (18)$$

and

$$\begin{aligned}
 M_\pm(k) &= (2\mu \pm V \cosh \beta + 2\Delta_2 \cos k), \\
 z(k) &= \Delta_1(1 + e^{-ik}),
 \end{aligned}$$

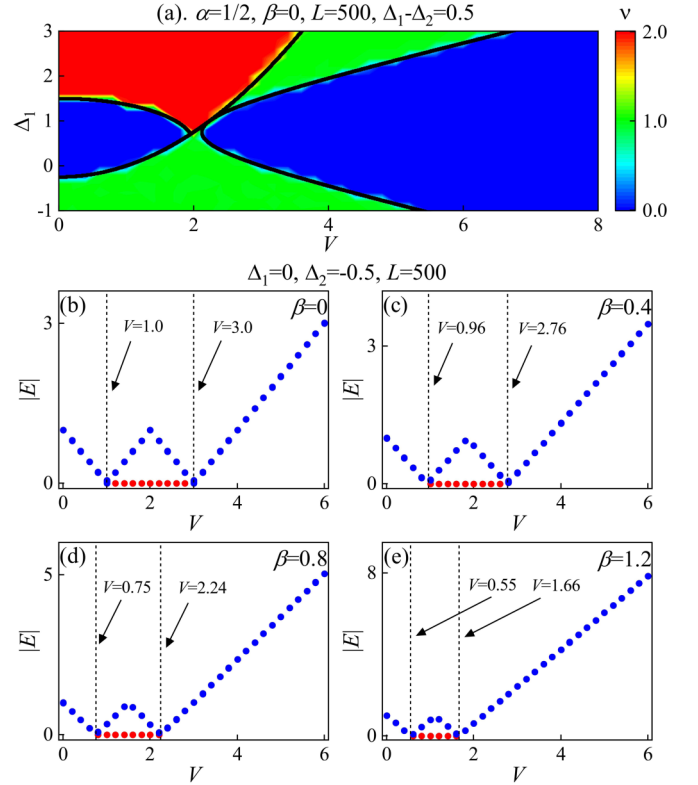


FIG. 6. (a) The real-space winding number ν as a function of the AAH potential strength V and Δ_1 ($\Delta_2 = \Delta_1 - 0.5$). The black solid lines are phase boundaries given by Eqs. (20) and (21). (b)–(e) Spectra under OBCs (only the energy levels with the ten smallest $|E|$ s are shown) as functions of the AAH potential strength V with $\Delta_1 = 0$, $\Delta_2 = -0.5$, and $\beta = 0, 0.4, 0.8, 1.2$ correspondingly. Red points are zero modes, and block dashed lines are phase boundaries given by Eqs. (20) and (21). Other parameters are lattice strength $L = 500$, the length of the boundary interval $l = 100$, and $\alpha = 1/2$.

$$\begin{aligned}
 w(k) &= \Delta_1(1 - e^{-ik}), \\
 q(k) &= -2i\Delta_2 \sin k. \quad (19)
 \end{aligned}$$

We can also obtain the winding number given by (see Appendix C)

$$\nu' = \frac{1}{2\pi i} \int_{-\pi}^{\pi} dk \partial_k \ln(\mu' + \Delta_1' e^{ik} + \Delta_2' e^{2ik}), \quad (20)$$

where

$$\begin{aligned}
 \mu' &= V^2 \cosh^2 \beta - 4\mu^2, \quad \Delta_1' = 4\Delta_1^2 - 8\mu\Delta_2, \\
 \Delta_2' &= -4\Delta_2^2. \quad (21)
 \end{aligned}$$

Note that Eq. (20) has a similar form as Eq. (6), we find that $\nu' = 1$ for $(\Delta_2' - \Delta_1' + \mu')(\Delta_2' + \Delta_1' + \mu') < 0$; $\nu' = 2$ for $(\Delta_2' - \Delta_1' + \mu')(\Delta_2' + \Delta_1' + \mu') > 0$ and $(\mu' - \Delta_2')(\Delta_2' \pm \Delta_1' + \mu') < 0$; $\nu' = 0$ for other cases. When $V = 0$, Eq. (16) reduces to Eq. (1), and we check that Eqs. (20) and (6) give the same phase diagrams in Appendix C.

In Fig. 6(a), we give the phase diagram and boundaries for $(\alpha, \beta) = (1/2, 0)$ and $\Delta_1 - \Delta_2 = 0.5$. We find that the commensurate AAH potential can also introduce the topological phases. (For example, $\nu = 0 \rightarrow 1$, $\nu = 0 \rightarrow 2$, and $\nu =$

2 → 1 without Anderson localization.) Besides, Fig. 6(a) indicates that topological regions induced by the $\alpha = 1/2$ AAH potential can be expressed as $f_1(\Delta_1) < V < f_2(\Delta_1)$ for a specific Δ_1 . Since imaginary phase shift $i\beta$ just leads to the replacement $V \rightarrow V \cosh \beta$ in phase boundaries [see Eq. (21)] and $\cosh \beta > 1$ when $\beta \neq 0$, the imaginary phase shift $-i\beta$ suppresses the corresponding topological region about V , which is also supported by results of spectra and corresponding phase boundaries under the OBCs with $(\Delta_1, \Delta_2) = (0, -0.5)$ and $\beta = 0, 0.4, 0.8, 1.2$ in Figs. 6(b)–6(e). At last, we also note that $V_n = -\cos(\pi n - i\beta) = \pm \cosh \beta$ is always Hermitian potentials for the $\alpha = 1/2$ case, so the suppression of the $\alpha = 1/2$ AAH potential-induced topological phase from the imaginary phase shift does not rely on the non-Hermiticity.

V. SUMMARY

To summarize, we discover the topological phases induced by commensurate ($\alpha = 1/2$) or incommensurate [$\alpha = (\sqrt{5} - 1)/2$] AAH potentials in the 1D longer-range spinless Kitaev chain. For the $\alpha = (\sqrt{5} - 1)/2$ case, we find the AAH potential-induced topological phases, and these topological phases are not always a topological Anderson phase; For the $\alpha = 1/2$ case, the AAH potential-induced topological phases can also exist in our model without Anderson localization. We also find that the imaginary phase shift can suppress the AAH potential-induced topological phases and leads the system to be more localized. These results could be helpful in further studies about topological phases with the longer-range interactions. Besides, since the 1D TSC with the next-nearest term is related to the transverse Ising model with three-spin interactions [12,14,15], our results might be also helpful to further studies about the related spin model and the local/nonlocal qubit with the (quasi)periodic fields. Finally, it is also valuable to simulate this model in some experimental systems including photonic systems [84], cold atom systems [31–33], and electric circuits [34].

ACKNOWLEDGMENTS

This work was supported by the State Key Program for Basic Researches of China under Grant No. 2017YFA0303203 (D.X.), and the National Natural Science Foundation of China under Grant No. 11974168 (L.S.).

APPENDIX A: WINDING NUMBER OF THE LONGER-RANGE KITAEV CHAIN WITHOUT THE AAH POTENTIAL

In this section, we discuss how to obtain the winding number of the longer-range Kitaev chain from Eq. (6). Note that

$$\begin{aligned} g_k &= \mu + \Delta_1 e^{ik} + \Delta_2 e^{2ik} \\ &= (\mu + \Delta_1 \cos k + \Delta_2 \cos 2k) \\ &\quad + i(\Delta_1 \sin k + \Delta_2 \sin 2k), \end{aligned} \quad (\text{A1})$$

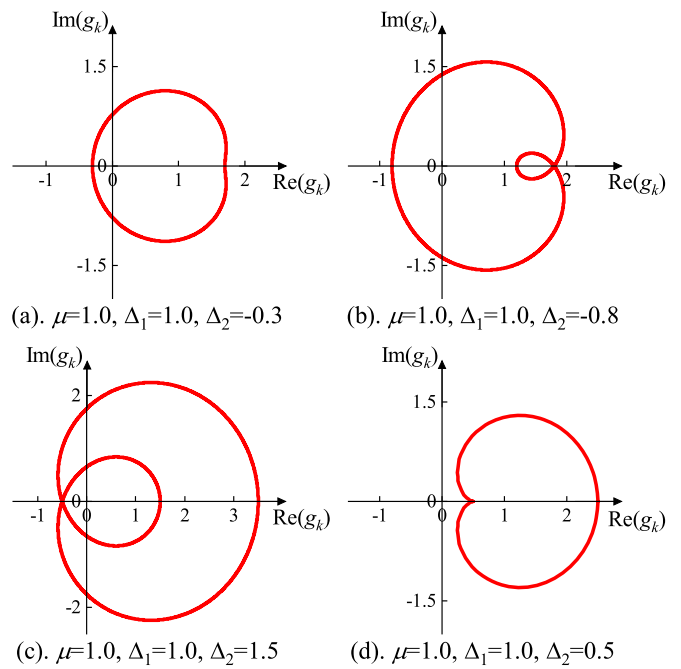


FIG. 7. Trajectories of g_k for several different cases in topological regions, the corresponding winding number ν is 1, 1, 2, and 0 in (a)–(d).

we have

$$\begin{aligned} g_0 &= \mu + \Delta_1 + \Delta_2, \\ g_\pi &= \mu - \Delta_1 + \Delta_2, \\ g_{k_0} &= \mu + \Delta_1 \cos k_0 + \Delta_2 \cos 2k_0 \\ &= \mu + \Delta_1 \cos k_0 + \Delta_2(2 \cos^2 k_0 - 1) \\ &= \mu - \Delta_2, \end{aligned} \quad (\text{A2})$$

where $\cos k_0 = -\Delta_1/(2\Delta_2)$. Since the winding number is identified by the trajectory of $g(k)$ on the complex plane (see examples in Fig. 7), we can obtain that $\nu = 1$ when $g_0 g_\pi < 0$; $\nu = 2$ when $g_0 g_\pi > 0, g_{k_0} g_\pi < 0$, and $g_{k_0} g_0 < 0$; $\nu = 0$ for other cases. Thus, we obtain the results from Eq. (6).

APPENDIX B: EFFECTS OF THE IMAGINARY PHASE SHIFT β IN TSC → AAH POTENTIAL-INDUCED TSC PHASE TRANSITION

In this section, we present the effects of the imaginary phase-shift β in the TSC → AAH potential-induced TSC phase transition in Fig. 8. Here we set $\Delta_1 = 2.5, \Delta_2 = 2.0$, and find that the topological phase with a larger AAH potential strength V is easier to be suppressed than the one with the smaller potential strength V : The $\nu = 2$ TSC phase is suppressed at first. Then, the $\nu = 1$ AAH potential-induced TSC phase is also suppressed. The boundaries in the $\nu = 2 \rightarrow 1$ transition are almost the same.

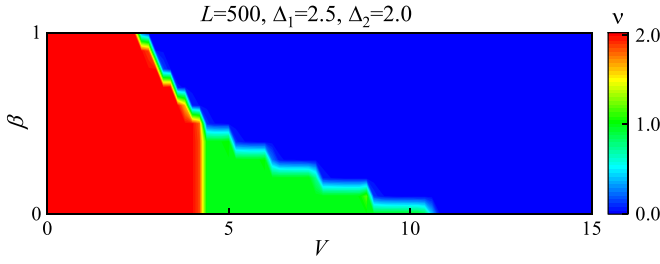


FIG. 8. The real-space winding number ν as a function of the AAH potential strength V and β with $\Delta_1 = 2.5$, $\Delta_2 = 2.0$. Other parameters are lattice strength $L = 500$, the length of the boundary interval $l = 100$, and $\alpha = [\sqrt{5} - 1]/2$.

APPENDIX C: WINDING NUMBER OF THE LONGER-RANGE KITAEV CHAIN WITH THE $\alpha = 1/2$ AAH POTENTIAL

In this Appendix, we give more details about the derivation of Eqs. (20) and (21) in the main text. Let us begin with Eq. (18) in the main text, To this end, we introduce the following unitary transformation:

$$U = \frac{1}{\sqrt{2}} \begin{pmatrix} 1 & 0 & 1 & 0 \\ 0 & 1 & 0 & 1 \\ -i & 0 & i & 0 \\ 0 & -i & 0 & i \end{pmatrix}. \quad (\text{C1})$$

After this transformation, we have

$$H'(k) = UH(k)U^{-1} = \begin{pmatrix} 0 & A_k^\dagger \\ A_k & 0 \end{pmatrix}, \quad (\text{C2})$$

with

$$A_k = i \begin{pmatrix} M_-(k) - q(k) & z(k) + w(k) \\ z^*(k) - w^*(k) & M_+(k) - q(k) \end{pmatrix}. \quad (\text{C3})$$

Then, we have

$$\begin{aligned} \nu' &= \frac{1}{2\pi i} \int_{-\pi}^{\pi} dk \partial_k \ln[\det(A_k)] \\ &= [z(k) + w(k)][z^*(k) - w^*(k)] \end{aligned}$$

$$\begin{aligned} &- [M_+(k) - q(k)][M_-(k) - q(k)] \\ &= \frac{1}{2\pi i} \int_{-\pi}^{\pi} dk \partial_k [\ln(\mu' + \Delta'_1 e^{ik} + \Delta'_2 e^{2ik})]. \quad (\text{C4}) \end{aligned}$$

where

$$\begin{aligned} M_{\pm}(k) &= (2\mu \pm V \cosh \beta + 2\Delta_2 \cos k), \\ z(k) &= \Delta_1(1 + e^{-ik}), \\ w(k) &= \Delta_1(1 - e^{-ik}), \\ q(k) &= -2i\Delta_2 \sin k. \end{aligned} \quad (\text{C5})$$

Then, we can obtain the results in the main text. i.e., $\nu' = 1$ for $(\Delta'_2 - \Delta'_1 + \mu')(\Delta'_2 + \Delta'_1 + \mu') < 0$; $\nu' = 2$ for $(\Delta'_2 - \Delta'_1 + \mu')(\Delta'_2 + \Delta'_1 + \mu') > 0$, $(\mu' - \Delta'_2)(\Delta'_2 \pm \Delta'_1 \pm \mu') < 0$; $\nu' = 0$ for the other case.

Next we check that Eqs. (20) and (6) in the main text give the same results when $V = 0$, we find that for $\nu' = 1$,

$$\begin{aligned} &(\Delta'_2 - \Delta'_1 + \mu')(\Delta'_2 + \Delta'_1 + \mu') \\ &= -16[\Delta_1^2 + (\Delta_2 - \mu)^2][\Delta_1^2 - (\Delta_2 + \mu)^2] < 0, \quad (\text{C6}) \end{aligned}$$

i.e.,

$$(\Delta_2 + \mu)^2 - \Delta_1^2 = (\Delta_2 - \Delta_1 + \mu)(\Delta_2 + \Delta_1 + \mu) < 0 \quad (\text{C7})$$

for $\nu = 2$, note that

$$\Delta'_2 - \Delta'_1 + \mu' = -4[\Delta_1^2 + (\Delta_2 - \mu)^2] < 0, \quad (\text{C8})$$

and

$$\begin{aligned} &(\mu' - \Delta'_2)(\Delta'_2 \pm \Delta'_1 + \mu') < 0, \\ &(\Delta'_2 - \Delta'_1 + \mu')(\Delta'_2 + \Delta'_1 + \mu') > 0, \quad (\text{C9}) \end{aligned}$$

we have

$$\begin{aligned} \Delta'_2 + \Delta'_1 + \mu' &= 4[\Delta_1^2 - (\Delta_2 + \mu)^2] < 0, \\ \mu' - \Delta'_2 &= -4(\mu^2 - \Delta_2^2) < 0, \quad (\text{C10}) \end{aligned}$$

which leads to

$$\Delta_2 > \mu, \quad (\Delta_2 - \Delta_1 + \mu)(\Delta_2 + \Delta_1 + \mu) > 0. \quad (\text{C11})$$

And $\nu' = 0$ for other cases. So Eqs. (20) and (6) in the main text lead to the same phase diagrams under the $V = 0$ limit.

-
- [1] E. Majorana, *Nuovo Cimento* **14**, 171 (1937).
 [2] N. Read and D. Green, *Phys. Rev. B* **61**, 10267 (2000).
 [3] D. A. Ivanov, *Phys. Rev. Lett.* **86**, 268 (2001).
 [4] C. Nayak, S. H. Simon, A. Stern, M. Freedman, and S. Das Sarma, *Rev. Mod. Phys.* **80**, 1083 (2008).
 [5] A. Y. Kitaev, *Phys.-Usp.* **44**, 131 (2001).
 [6] J. Alicea, *Rep. Prog. Phys.* **75**, 076501 (2012).
 [7] M. Z. Hasan and C. L. Kane, *Rev. Mod. Phys.* **82**, 3045 (2010).
 [8] X.-L. Qi and S. C. Zhang, *Rev. Mod. Phys.* **83**, 1057 (2011).
 [9] R. M. Lutchyn, J. D. Sau, and S. Das Sarma, *Phys. Rev. Lett.* **105**, 077001 (2010).
 [10] Y. Oreg, G. Refael, and F. von Oppen, *Phys. Rev. Lett.* **105**, 177002 (2010).
 [11] V. Mourik, K. Zuo, S. M. Frolov, S. R. Plissard, E. P. A. M. Bakkers, and L. P. Kouwenhoven, *Science* **336**, 1003 (2012).
 [12] Y. Niu, S. B. Chung, C.-H. Hsu, I. Mandal, S. Raghu, and S. Chakravarty, *Phys. Rev. B* **85**, 035110 (2012).
 [13] S. Lieu, D. K. K. Lee, and J. Knolle, *Phys. Rev. B* **98**, 134507 (2018).
 [14] A. Habibi, S. A. Jafari, and S. Rouhani, *Phys. Rev. B* **98**, 035142 (2018).
 [15] P. Smacchia, L. Amico, P. Facchi, R. Fazio, G. Florio, S. Pascazio, and V. Vedral, *Phys. Rev. A* **84**, 022304 (2011).
 [16] B. Pérez-González, M. Bello, A. Gómez-León, and G. Platero, *Phys. Rev. B* **99**, 035146 (2019).
 [17] H.-C. Hsu and T.-W. Chen, *Phys. Rev. B* **102**, 205425 (2020).
 [18] A. C. Potter and P. A. Lee, *Phys. Rev. Lett.* **105**, 227003 (2010).
 [19] L.-J. Lang and S. Chen, *Phys. Rev. B* **86**, 205135 (2012).
 [20] X. Cai, L.-J. Lang, S. Chen, and Y. Wang, *Phys. Rev. Lett.* **110**, 176403 (2013).

- [21] W. DeGottardi, D. Sen, and S. Vishveshwara, *Phys. Rev. Lett.* **110**, 146404 (2013).
- [22] W. DeGottardi, D. Sen, and S. Vishveshwara, *New J. Phys.* **13**, 065028 (2011).
- [23] J. Wang, X.-J. Liu, G. Xianlong, and H. Hu, *Phys. Rev. B* **93**, 104504 (2016).
- [24] Q.-B. Zeng, S. Chen, and R. Lü, *Phys. Rev. B* **94**, 125408 (2016).
- [25] Q.-B. Zeng, S. Chen, and R. Lü, *New J. Phys.* **20**, 053012 (2018).
- [26] X. Tong, Y.-M. Meng, X. Jiang, C. Lee, G. Dias de Moraes Neto, and G. Xianlong, *Phys. Rev. B* **103**, 104202 (2021).
- [27] T. Lv, T.-C. Yi, L. Li, G. Sun, and W.-L. You, *Phys. Rev. A* **105**, 013315 (2022).
- [28] I. Rotter, *J. Phys. A: Math. Theor.* **42**, 153001 (2009).
- [29] B. Zhen, C. W. Hsu, Y. Igarashi, L. Lu, I. Kaminer, A. Pick, S.-L. Chua, J. D. Joannopoulos, and M. Soljačić, *Nature (London)* **525**, 354 (2015).
- [30] S. Malzard, C. Poli, and H. Schomerus, *Phys. Rev. Lett.* **115**, 200402 (2015).
- [31] Y. Xu, S.-T. Wang, and L.-M. Duan, *Phys. Rev. Lett.* **118**, 045701 (2017).
- [32] J. Li, A. K. Harter, J. Liu, L. de Melo, Y. N. Joglekar, and L. Luo, *Nat. Commun.* **10**, 855 (2019).
- [33] L. Zhou, *Phys. Rev. B* **101**, 014306 (2020).
- [34] M. Ezawa, *Phys. Rev. B* **100**, 045407 (2019).
- [35] S. Liu, S. Ma, C. Yang, L. Zhang, W. Gao, Y. J. Xiang, T. J. Cui, and S. Zhang, *Phys. Rev. Appl.* **13**, 014047 (2020).
- [36] H. Zhou, C. Peng, Y. Yoon, C. W. Hsu, K. A. Nelson, L. Fu, J. D. Joannopoulos, M. Soljacic, and B. Zhen, *Science* **359**, 1009 (2018).
- [37] L. Feng, Z. J. Wong, R.-M. Ma, Y. Wang, and X. Zhang, *Science* **346**, 972 (2014).
- [38] H. Hodaei, M.-A. Miri, M. Heinrich, D. N. Christodoulides, and M. Khajavikhan, *Science* **346**, 975 (2014).
- [39] V. Kozii and L. Fu, [arXiv:1708.05841](https://arxiv.org/abs/1708.05841).
- [40] A. A. Zyuzin and A. Y. Zyuzin, *Phys. Rev. B* **97**, 041203(R) (2018).
- [41] M. Papaj, H. Isobe, and L. Fu, *Phys. Rev. B* **99**, 201107(R) (2019).
- [42] E. J. Bergholtz and J. C. Budich, *Phys. Rev. Research* **1**, 012003(R) (2019).
- [43] E. J. Bergholtz, J. C. Budich, and F. K. Kunst, *Rev. Mod. Phys.* **93**, 015005 (2021).
- [44] J. Carlström and E. J. Bergholtz, *Phys. Rev. A* **98**, 042114 (2018).
- [45] Z. Yang and J. Hu, *Phys. Rev. B* **99**, 081102(R) (2019).
- [46] Y.-H. Lai, Y.-K. Lu, M.-G. Suh, Z. Yuan, and K. Vahala, *Nature (London)* **576**, 65 (2019).
- [47] H. Hodaei, A. U. Hassan, S. Wittek, H. Garcia-Gracia, R. El-Ganainy, D. N. Christodoulides, and M. Khajavikhan, *Nature (London)* **548**, 187 (2017).
- [48] S. Yao, F. Song, and Z. Wang, *Phys. Rev. Lett.* **121**, 136802 (2018).
- [49] S. Yao and Z. Wang, *Phys. Rev. Lett.* **121**, 086803 (2018).
- [50] L. Xiao, T. Deng, K. Wang, G. Zhu, Z. Wang, W. Yi, and P. Xue, *Nat. Phys.* **16**, 761 (2020).
- [51] K. Yokomizo and S. Murakami, *Phys. Rev. Lett.* **123**, 066404 (2019).
- [52] H. Wang, J. Ruan, and H. Zhang, *Phys. Rev. B* **99**, 075130 (2019).
- [53] Y. Xiong, *J. Phys. Commun.* **2**, 035043 (2018).
- [54] Y. Yi and Z. Yang, *Phys. Rev. Lett.* **125**, 186802 (2020).
- [55] K. Zhang, Z. Yang, and C. Fang, *Phys. Rev. Lett.* **125**, 126402 (2020).
- [56] Z. Yang, K. Zhang, C. Fang, and J. Hu, *Phys. Rev. Lett.* **125**, 226402 (2020).
- [57] L. Li, C. H. Lee, S. Mu, and J. Gong, *Nat. Commun.* **11**, 5491 (2020).
- [58] N. Okuma and M. Sato, *Phys. Rev. Lett.* **123**, 097701 (2019).
- [59] A. Basiri, Y. Bromberg, A. Yamilov, H. Cao, and T. Kottos, *Phys. Rev. A* **90**, 043815 (2014).
- [60] X. Cai, *Phys. Rev. B* **103**, 014201 (2021).
- [61] Y. Liu, X.-P. Jiang, J. Cao, and S. Chen, *Phys. Rev. B* **101**, 174205 (2020).
- [62] Y. Liu, Y. Wang, X.-J. Liu, Q. Zhou, and S. Chen, *Phys. Rev. B* **103**, 014203 (2021).
- [63] Q.-B. Zeng, S. Chen, and R. Lü, *Phys. Rev. A* **95**, 062118 (2017).
- [64] Q.-B. Zeng, Y.-B. Yang, and Y. Xu, *Phys. Rev. B* **101**, 020201(R) (2020).
- [65] S. Longhi, *Phys. Rev. B* **100**, 125157 (2019).
- [66] S. Longhi, *Phys. Rev. Lett.* **122**, 237601 (2019).
- [67] T. Liu, H. Guo, Y. Pu, and S. Longhi, *Phys. Rev. B* **102**, 024205 (2020).
- [68] Y. Liu, Q. Zhou, and S. Chen, *Phys. Rev. B* **104**, 024201 (2021).
- [69] H. Jiang, L.-J. Lang, C. Yang, S.-L. Zhu, and S. Chen, *Phys. Rev. B* **100**, 054301 (2019).
- [70] T. Liu, S. Cheng, H. Guo, and G. Xianlong, *Phys. Rev. B* **103**, 104203 (2021).
- [71] X. Cai, *Phys. Rev. B* **103**, 214202 (2021).
- [72] Z.-H. Wang, F. Xu, L. Li, D.-H. Xu, and B. Wang, *Phys. Rev. B* **104**, 174501 (2021).
- [73] Z.-H. Wang, F. Xu, L. Li, D.-H. Xu, and B. Wang, *Phys. Rev. B* **105**, 024514 (2022).
- [74] P. W. Anderson, *Phys. Rev.* **109**, 1492 (1958).
- [75] S. Aubry and G. André, *Ann. Isr. Phys. Soc.* **3**, 133 (1980).
- [76] J. Li, R.-L. Chu, J. K. Jain, and S.-Q. Shen, *Phys. Rev. Lett.* **102**, 136806 (2009).
- [77] C. W. Groth, M. Wimmer, A. R. Akhmerov, J. Tworzydło, and C. W. J. Beenakker, *Phys. Rev. Lett.* **103**, 196805 (2009).
- [78] H. Jiang, L. Wang, Q.-F. Sun, and X. C. Xie, *Phys. Rev. B* **80**, 165316 (2009).
- [79] J. Borchmann, A. Farrell, and T. Pereg-Barnea, *Phys. Rev. B* **93**, 125133 (2016).
- [80] K. Kawabata, K. Shiozaki, M. Ueda, and M. Sato, *Phys. Rev. X* **9**, 041015 (2019).
- [81] F. Song, S. Yao, and Z. Wang, *Phys. Rev. Lett.* **123**, 246801 (2019).
- [82] D.-W. Zhang, L.-Z. Tang, L.-F. Lang, H. Yuan, and S.-L. Zhu, *Sci. China: Phys., Mech. Astron.* **63**, 267062 (2020).
- [83] X.-W. Luo and C. Zhang, [arXiv:1912.10652](https://arxiv.org/abs/1912.10652).
- [84] J. S. Xu, K. Sun, Y. J. Han, C. F. Li, J. K. Pachos, and G. C. Guo, *Nat. Commun.* **7**, 13194 (2016).